Desantes Fernández, JM.; García Oliver, JM.; Vera-Tudela-Fajardo, WM.; López Pintor, D.; Schneider, B.; Boulouchos, K. (2016). Study of the auto-ignition phenomenon of PRFs under HCCI conditions in a RCEM by means of spectroscopy. Applied Energy. 179:389-400. doi:10.1016/j.apenergy.2016.06.134.

Study of the auto-ignition phenomenon of PRFs under HCCI conditions in a RCEM by means of spectroscopy

J.M. Desantes[a], J.M. García-Oliver[a], W. Vera-Tudela[a,b,*], D. López-Pintor[a,b,*], B. Schneider[b], K. Boulouchos[b]

[a] *CMT-Motores Térmicos*
Universitat Politècnica de València
Camino de Vera, s/n. 46022 Valencia, SPAIN
[b] *Laboratorium für Aerothermochemie und Verbrennungssysteme*
Eidgeössiche Technische Hochschule Zürich
Sonneggstrasse 3,CH-8092 Zürich, SWITZERLAND

Abstract

An investigation of the effects of contour conditions and fuel properties on the auto-ignition and combustion process under HCCI conditions is presented in this study. A parametric variation of initial temperature, intake pressure, compression ratio, oxygen concentration and equivalence ratio has been carried out for Primary Reference Fuels in a Rapid Compression Expansion Machine while applying spectroscopy. The results have also been contrasted with natural chemiluminescence measurements. Additionally, the experiments have been simulated in CHEMKIN and the results derived from the optical techniques have been compared with the results from the chemical kinetics of the process, validating the chemical kinetic mechanism and an additional sub-model of excited OH^*. Two different scenarios can be seen according to the results from the spectrograph. For very lean or very low-

*Corresponding author
Tel: +34 963 879 232. Fax: +34 963 877 659. E-mail: *walvetu@mot.upv.es*
dalopin1@mot.upv.es

temperature combustions no peak of OH^* is seen at $310nm$ of wavelength, proving that the luminosity came from the CO continuum rather than from the OH^*. However, for more intense combustions (richer equivalence ratios, higher temperatures or lower EGR rates) spectrography shows a clear peak of OH^* that has much longer time of life than the corresponding to the CO continuum. The main chemical reaction that causes this two scenarios has been identified as $H + HO_2 \Rightarrow 2OH$. The increase of relevance of this reaction at high combustion temperatures causes a higher OH^* accumulation, which leads to a brighter OH^* emission. Finally, for low temperature combustions the CO continuum out-shines the OH^* radiation so the light emitted by this radical cannot be detected by means of natural chemiluminescence.
Keywords: RCEM, spectroscopy, PRF, chemiluminescence

1. Introduction

Homogeneous Charge Compression Ignition (HCCI), Premixed Charge Compression Ignition (PCCI) and other advanced engine combustion modes based on Low Temperature Combustion (LTC), have been studied in the last years as ways to simultaneously reduce soot and NO_x emissions in Compression Ignition (CI) engines [1, 2]. These modes manage to accomplish such task; however, high emissions of unburned hydrocarbons (UHC) and carbon monoxide (CO) are achieved. The reduction of soot and NO_x are reached by avoiding their formation peninsulas, which can be seen in equivalence ratio - temperature diagrams [3]. UHC and CO can be easily oxidized with the current post-treatment systems. Thus, the main challenge to implement these new combustion strategies in commercial reciprocating internal combustion

engines is the lack of control over the autoignition process and over the heat release rate [4].

The ignition control is much more difficult under these conditions; however, by adjusting engine operating parameters like the Exhaust Gas Recirculation (EGR) rate or the inlet temperature, the chemical kinetics of the charge can be controlled [5]. Therefore, it is necessary to improve the knowledge about the autoignition phenomenon and about the combustion process under low temperature conditions to properly modify the operating conditions of the engine and control the heat release and, therefore, the combustion efficiency.

Spectroscopy is a non-intrusive optical technique widely used in combustion diagnosis [6], such optical techniques are powerful tools to analyze not only the ignition of homogeneous mixtures, but also different parameters of the combustion process. Natural luminosity analysis and spectroscopy have shown to be able to describe the different phases of the combustion process under HCCI conditions [7].

Mancaruso and Vaglieco [8] applied spectroscopic measurements to a transparent diesel engine in order to study the low temperature combustion process. They saw that the OH^* was widely distributed in the chamber during the whole combustion process, concluding that OH^* was recognized as the most important radical that marked premixed combustions.

Iijima and Shoji [9] also performed a spectroscopic analysis of HCCI combustion for *n*-heptane and *iso*-octane in a 2-stroke single-cylinder engine. The authors found that the time of the peak light emission intensity in a wavelength range of 300 - 500 nm nearly coincides with the time of the peak

of heat release rate, which could be used as a tracer of the high temperature ignition delay. However, no light emission spectrum attributable to cool flames was observed at high EGR rates. Moreover, a strong and long-lived light emission attributable to the OH^* radical can be seen only under high equivalence ratios.

Kim et al. [10] compared the HCCI mode with PCCI and standard spark ignition (SI) using spectrum analysis, with a transparent engine. The authors found that the $CO - O^*$ emission dominates the spectra in the HCCI chemiluminescence emission, but it is difficult to measure OH^*, CH^*, and ${C_2}^*$ radicals. Moreover, the presence of OH^* peaks in the spectra of very lean HCCI combustion could be an indication of non-homogeneous conditions. The authors concluded that chemiluminescence is as a good method for analyzing engine combustion.

Murase et al. [11] have studied the HCCI combustion with a Rapid Compression Machine by means of direct visualization and spectroscopy. They could see that during the main heat release duration the distinct OH^* emission appeared, and it was superimposed on the carbon monoxide oxidation continuum. After the main heat release, the broad peak of the spectrum was shifted to the longer-wavelength side (H_2O vibration-rotation bands at 580.7 - 966.9 nm).

Finally, Hwang et al. [12] studied the temporal phases of autoignition and combustion in an HCCI optical engine for several fuels by applying a spectroscopic and a chemical-kinetic analysis. The authors divide the combustion process in four different stages, which can be described by spectroscopy: Low-temperature heat-release phase or cool flames (only existing

in two-stage ignition process), intermediate-temperature heat-release phase (which affects the fuel ignition quality), main high-temperature heat-release phase and, finally, a burnout phase (with very weak uniform emission and near-zero heat-release rate).

The motivation of this study is the analysis of the combustion under HCCI conditions in order to extend the aforementioned studies. The spectra of homogeneous combustions is now analysed under a wider range of conditions, extending the studies of Iijima and Shoji [9] to different equivalence ratios, compression ratios, initial temperatures and pressures and EGR rates. The importance of studying the combustion ignition delay time under HCCI conditions is justified by the role of this parameter in controlling the heat release rate and the efficiency under such conditions. The optical analysis contributes by studying the sources of the radiation and which chemical reactions control them. Furthermore, a more complete sub-model of excited OH has been validated with experimental results, not only referred to the ignition delay time of OH^* but also the *time of life* of the radicals. This sub-model has been developed based on the Hall and Petersen sub-model for the OH^* [13], extending the number of reactions involved. The validation of such sub-model in a broad range of operating conditions allows the use of the mechanism in future works of research.

In this study autoignition and combustion are studied under HCCI conditions in a Rapid Compression Expansion Machine (RCEM) by means of spectroscopy. The study has been performed with two different surrogate fuels with reactivities typical of diesel fuel and gasoline: *n*-heptane and *iso*-octane, respectively. Despite the fact that more sophisticated surrogate fuels

for diesel and gasoline can be found in the literature, *n*-heptane and *iso*-octane were chosen because extended and fully validated chemical kinetic mechanisms are available for both of them. Moreover, *n*-heptane, *iso*-octane and their blends are Primary Reference Fuels (PRF) employed to define the octane reference scale and they are widely used in the literature as surrogates of diesel and gasoline under engine conditions [14].

Spectra of the combustion process and chemiluminescent intensity distribution will be experimentally obtained under different conditions of pressure, temperature, equivalence ratio and oxygen mass fraction. Experiments are reproduced with the software of chemical simulation CHEMKIN. This software, which is developed by Reaction Design (ANSYS), is consolidated in the world of engineering investigations [15] and the chemical kinetics mechanisms of several hydrocarbons are perfectly defined to be used with it [16]. Finally, the numerical results are validated experimentally using a RCEM.

The structure of the paper is as follows:

- The experimental facilities involved in the study are presented, including the RCEM and the additional optical setup.
- The methodological approach is detailed, where the experimental and simulation methods are described and the parametric study performed is presented.
- The main chemical kinetic mechanism and the sub-model for the excited OH at an excited estate are presented and validated by comparison with experimental results.
- Results are presented from a spectroscopy point of view, linking the

optical results with different stages of the process.

- Finally, the conclusions of this study are shown.

2. Experimental tools

2.1. Rapid Compression Expansion Machine

A RCEM is an experimental facility widely used in autoignition studies due to its capability to reproduce engine conditions [17]. It can replicate the combustion process of reciprocating engines with fully controlled initial and boundary conditions and avoiding the complexities associated to engines [18].

Different compression ratios can be achieved in the RCEM by varying the stroke and the clearance volume. Axial optical access is available [19] and the compression velocity can be varied in order to simulate the effect of different engine speeds. In a RCEM part of the expansion stroke of the piston can be also analyzed and most of the engine parameters can be calculated, such as the heat release rate or the combustion efficiency. In this facility both homogeneous and heterogeneous (direct injection) mixtures can be tested, as well as new combustion modes such as the dual fuel technology [20] or LTC [21].

A schematic of the RCEM is shown in Figure 1. The RCEM is pneumatically driven and its pistons are hydraulically coupled. As it can be seen, it can be divided in two different zones, the experimentation zone and the driving zone. The experimentation zone is composed by the combustion chamber, while the driving zone is composed by four different pistons. Piston 1, which is called pushing piston, is pneumatically driven and hydraulically coupled

to piston 2, which is called driver piston and is directly connected with the combustion chamber. Piston 3 is hydraulically driven and it can be adjusted to select the compression stroke. Finally, piston 4 contains the compressed air that drives the machine. Details on the operation principle of the RCEM can be found in [22].

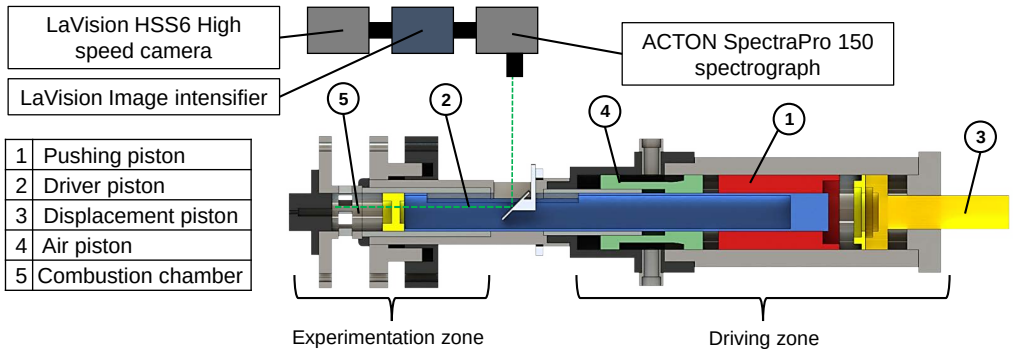

Figure 1: Rapid Compression Expansion Machine schematic.

The technical characteristics of the RCEM can be seen in Table 1. The pushing piston and the driver piston are instrumented with two incremental position sensors (AMO LMK102) with a resolution of 0.01 mm, which allow knowing the absolute position of each piston and; therefore, the combustion chamber volume. The combustion chamber is composed by three elements, the experimentation piston (mechanically connected to the driver piston), the liner and the cylinder head. The experimentation piston consists on a steel-made piston with 84 mm of bore and a quartz-made bowl with cylindrical shape, 50 mm of bore and 2.2 mm of depth, which allows the axial optical access. As the bowl is flat, the chamber images can be recorded without any

image distortion.

Bore	84	mm
Stroke	120 - 249	mm
Compression ratio	5 - 30	: 1
Maximum cylinder pressure	200	bar
Initial pressure	1 - 5	bar
Maximum heating temperature	473	K

Table 1: Technical characteristics of the RCEM.

Besides, the cylinder head and the cylinder liner have different heating elements arranged in six separately controlled zones, which are responsible for heating the cylinder walls and the experimentation piston. The wall temperature is measured by a total of six type K thermocouples, two located in the cylinder head and four in the liner. Very good temperature homogeneity has been observed [22], with a standard deviation of the gas temperature in the order of 3 K. It was found that the distribution of temperature is barely affected by the gas in-flow due to its slow speed. An initial gas temperature equal to the wall temperature is achieved due to the long duration of the intake process.

The cylinder head is instrumented with a Kistler 7061B cooled piezoelectric pressure sensor (-80 pC/bar of sensitivity), which is coupled to a Kistler 5011 charge amplifier, and whereby the in-cylinder pressure is measured. Different piezo-resistive pressure sensors are available to control the filling of the driving gas and of the combustion chamber (0.01 bar of resolution). The

injection system is composed by a Siemens hollow cone piezo-injector with a cone angle of 90°, which is centered in the cylinder head. Its fuel delivery rate has been previously measured with an IAV injection rate analyzer. The transient signals have been recorder at 100 kHz with a PC-based transient measurement recorder. The RCEM is filled from an external tank that can be heated up to 37 $3K$. The synthetic air is produced in the tank by a filling based on partial pressures where N_2, CO_2 and O_2 can be used. The mixture is analyzed in a Horiba PG-250 portable gas analyzer in order to know the exact composition and ensure the correct reproduction of the experiments in CHEMKIN.

2.2. Optical setup

A schematic of the optical arrangement is shown in Figure 1. Passive spectroscopy measurements were performed with an Acton SpectraPro150 spectrograph (grating: 150 g/mm, blaze wavelength: 500 nm) coupled with a 12-bit LaVision HighSpeedStar 6 camera and a LaVision HighSpeed IRO intensifier. The spectrograph has been pointed directly at the mirror inside the machine, which due to its 45° tilt gives a direct view of the combustion chamber through the piston window. Because of the transient nature of the combustion, an acquisition frequency of 67.5 kHz has been chosen in order to capture the evolution of the spectra inside de combustion chamber. An exposure time of 14.5 μs and a rectangular image of 1024x80 pixels were selected. The whole system was calibrated by the use of an Acton MS-416 mercury lamp.

Finally, natural chemiluminescence results have been used in order to analyze the combustion process. Such results were obtained coupling a 12-

bit LaVision HighSpeedStar6 camera with a LaVision HighSpeed IRO intensifier (acquisition frequency: 30 kHz, exposure time: 33 μs, resolution 384x448 pixels). A 310 nm interference filter (FWHM = 10 nm) was used to eliminate any additional radiation outside the OH^* radical wavelength.

The transient pressure and piston position along with control and synchronization signals (i.e. camera triggers) have been recorder at 100 kHz with a PC-based transient measurement recorder.

3. Methodological approach

3.1. Rapid Compression Expansion Machine

The desired stroke of the machine is selected and the RCEM is heated up to the desired temperature. Then, the synthetic air-EGR mixture is prepared in the mixing tank. In this study, EGR was considered as a combination of 20 % CO_2 + 80 % N_2 in volume, and it is mixed with dry air until the amount of oxygen in the mixture is the one desired by the user.

The combustion chamber is scavenged several times before the filling. The fuel is injected into the combustion chamber at the start of the intake process to avoid problems of stratification or other inhomogeneities. The long duration of the process (approximately 40 s), are enough to guarantee a homogeneous environment in the chamber when the compression stroke starts.

In order to ensure a representative ignition delay time measurement the number of repetitions of each point has been selected so that the semi-amplitude of the confidence interval with a level of confidence of 95 % is smaller than 1 % of the mean ignition delay value. The repeatability of the

machine has been previously studied in series of 10 repetitions under motoring conditions and under combustion conditions. The following maximum coefficients of variation have been found:

	Max. position	Time of max. pos.	Max. pressure	Time of max. press.
CV [%]	0.08	0.27	1.35	0.10

In this work the autoignition of the mixture is considered to be produced when the time derivative of the pressure signal (which will be referred as pressure rise rate or, simply, pressure rise further on) reaches a maximum. Thus, the ignition delay in the experimental facility is defined as the time between the start of the rapid compression process and the instant in which the maximum pressure rise is obtained, as can be seen in Figure 2. This way, cool flames and high temperature ignition delay can be easily distinguished in case of two-stage ignition.

Finally, the temperature profile is calculated for each experiment by applying the energy equation, since the pressure profile and the position of the piston are known. The heat losses are characterized by a model based on the Woschni correlation [23]. The calculation includes two additional models for deformations and leaks, both of them explained in [24, 25].

3.2. Spectrography

The spectral information has been obtained by processing the images captured with the intensifier-camera group coupled to the spectrograph. An in-house routine developed in MATLAB has been used to calculate the spectral evolution along time. The fluctuations and noise are smoothed by averaging

the 80 vertical pixels of each image, in this way the 2D image is reduced to a 1D vector with the intensity per each wavelength.

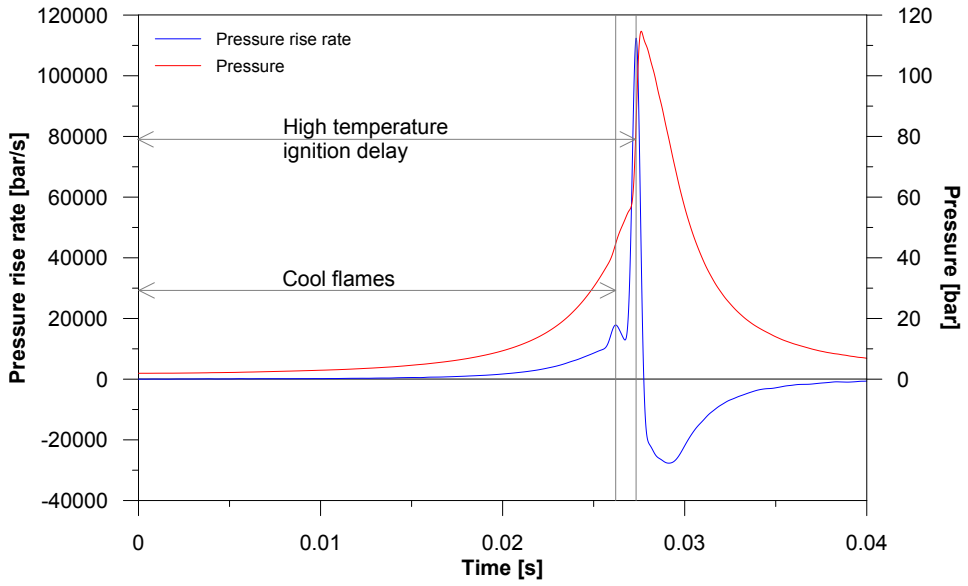

Figure 2: Ignition delay definition. The autoignition of the mixture is considered to be produced when the maximum pressure rise occurs. n-heptane at CR 17:1, T_i 358 K, EGR 47 % and Fr 0.58.

Figure 3 shows the result of the processing routine, it can be seen that the spectral information is resolved in the horizontal axis and that the vertical one is used as a filter for noise and oscillations. Finally, what is represented in plot is the calibration of the spectrograph with a mercury lamp from which the linear relationship between pixel and wavelength is deducted with a R^2 coefficient of 1, approximately.

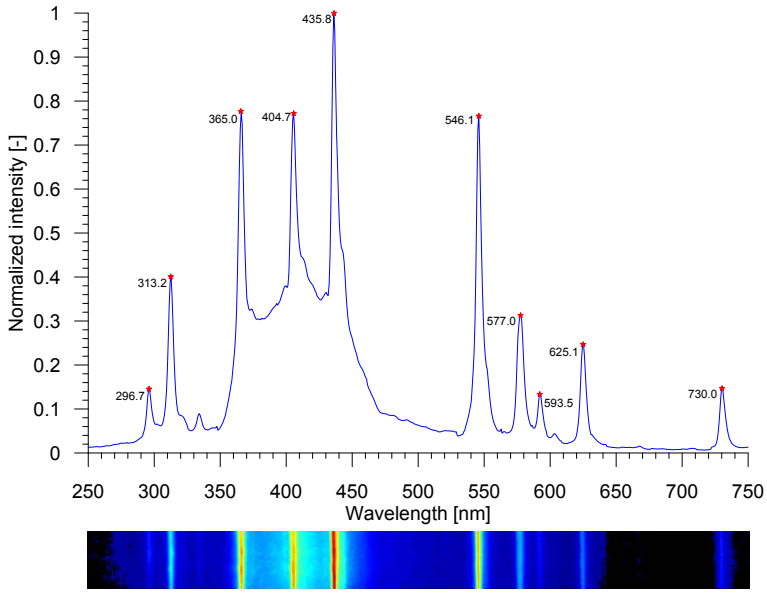

Figure 3: Spectral information of a sample image.

3.3. Chemical kinetic mechanisms

As previously mentioned, CHEMKIN is the software used to reproduce the experiments; the version used is CHEMKIN-PRO. Curran's kinetic mechanism is used for *n*-heptane and *iso*-octane [26, 27]. This mechanism consists of 1034 species and 4238 reactions, and includes the chemical kinetics of the two hydrocarbons used in this investigation. Its validity has been checked in several articles by comparison with experimental results [14, 28]. Additionally, the chemical mechanism has been modified to incorporate an OH^* sub-mechanism in order to be able to compare the chemiluminescence results in a easy way [13]. Furthermore, since the Curran chemical kinetics mechanism does not distinguish between OH (ground estate) and OH^* (excited estate) the main generation reactions of excited OH have been located and

modified in order to take into account the coexistence of both species [29]. The complete OH^* sub-model is explained in Appendix A.

The model used to obtain ignition delay times under variable conditions is a reciprocating internal combustion engine operating with homogeneous charge (IC-engine, closed 0-D reactors from CHEMKIN). The volume profile as well as the heat loss profile are imposed in order to reproduce the RCEM conditions. The piston starts at bottom dead center (BDC) and a complete cycle of the RCEM is simulated. The autoignition is considered to be produced when the time derivative of the pressure signal reaches a maximum. This is the same criterion as the one used in the experiments, and the comparison of ignition delay times between experimental and simulated results is how the mechanism was validated. Moreover, the OH, OH^*, CO and CO_2 concentration profiles are obtained and an analysis of their reaction rates has been performed in order to compare the simulations with the results obtained from the spectrograph. This way, the combustion phenomenon can be studied from a point of view of chemical kinetics. The maximum time step for CHEMKIN simulations has been set as 10^{-5} s which is the experimental resolution of the pressure signal.

3.4. Parametric study performed

The performed experimental study was as follows:

- Fuel: *n*-heptane and *iso*-octane.
- Initial temperature (T_i): 358 K (only for n-heptane), 383 K, 408 K, 433 K and 458 K.
- Initial pressure (P_i): 0.14 MPa and 0.17 MPa.

- Compression stroke: 249 mm.
- Compression ratio (CR): 15 and 17 to 1.
- Oxygen mass fraction (Y_{O_2}): 0.23 (0 % EGR), 0.147 (30 % EGR), 0.126 (40 % EGR) and 0.105 (50 % EGR).
- Equivalence ratio (Fr): 0.3 to 0.8 depending on the fuel and on the oxygen mass fraction.

The expected pressure and temperature at TDC under motoring conditions for these initial operating points are summarized in Table 2.

CR 15:1		**CR 17:1**	
T_i $[K]$	T_{TDC} $[K]$	T_i $[K]$	T_{TDC} $[K]$
358	874	358	911
383	936	383	975
408	997	408	1039
433	1058	433	1102
458	1119	458	1166
P_i $[MPa]$	P_{TDC} $[MPa]$	P_i $[MPa]$	P_{TDC} $[MPa]$
0.14	5.13	0.14	6.06
0.17	6.23	0.17	7.36

Table 2: Pressure and temperature conditions at TDC under motoring conditions for the initial operating points.

The maximum equivalence ratio is limited by the working oxygen mass fraction in order to avoid extremely violent combustions. The equivalence

ratio of 0.4 has been chosen as the base point in order to have the possibility to try leaner and richer mixtures without damaging the facility. The performed parametric study can be seen in Table 3. Finally, the temperature of the combustion chamber is always above the boiling point of the fuel, therefore ensuring that the fuel is in vapour phase before the beginning of the cycle.

		$\mathbf{T}_i$ [K]				
		358	**383**	**408**	**433**	**458**
Fr [-]	**0.3**	40		0, 30, 40, 50		40
	0.4	0, 30, 40, 50	40, 50	0, 30, 40, 50	40, 50	0, 30, 40, 50
	0.5	40	40	40, 50	40	40
	0.6	40		40, 50		40
	0.7			40, 50		
	0.8			40, 50		

Table 3: Parametric study performed. EGR percent for different initial temperatures and equivalence ratios. Black.- common points. Blue.- exclusively for *n*-heptane. Red.- exclusively for *iso*-octane.

4. Chemical kinetic mechanism and OH^* sub-model

In this section, the validity of the chemical kinetic mechanism the sub-model for the excited OH at an excited estate are checked by comparing them directly with the experimental results.

4.1. Validation of the chemical mechanism

Ignition delay times obtained solving the *n*-heptane and *iso*-octane detailed chemical kinetic mechanism are compared with the experimental re-

sults as a method to validate the mechanism in the desired range.

The percentage deviation in ignition delay (ϵ), was calculated in order to compare more easily experimental and simulation results. This deviation is defined as follows:

$$\epsilon = \frac{t_{SOC,ICE} - t_{SOC,RCEM}}{t_{SOC,RCEM}} \times 100$$

where t_{SOC} represents the start of combustion time. The subscript ICE represents a data obtained from a chemical simulation with CHEMKIN using a closed 0D ICE reactor. Finally, the subscript $RCEM$ represents a data obtained experimentally from the RCEM.

The average of the deviations in absolute value, $\bar{\epsilon} = \sum \mid \epsilon \mid /n$, has been calculated for each fuel. The confidence interval for the mean deviation with a confidence level of 95 % is equal to $[1.33, 1.98]$ % for n-heptane and to $[1.21, 1.89]$ % for *iso*-octane. Ignition delay deviations are caused partly by the chemical kinetic mechanism used and partly by the uncertainties in the calculation of the effective volume and the heat losses of the RCEM. The results show that simulations are able to reproduce the experimental ignition delays with quite good accuracy.

4.2. Validation of the OH sub-model*

Two additional ignition delays were defined: referred to a maximum oxidation rate of $CO + O \Rightarrow CO_2 + hv$, which is an estimator of the CO continuum, and referred to a maximum concentration of OH^*, which is an estimator of the OH^* chemiluminescence. Both ignition delays are obtained experimentally from the high speed camera and by simulation from CHEMKIN. The

percentage error in the ignition delay (ε), was calculated in order to compare more easily experimental and simulation results. This error is defined as follows:

$$\varepsilon = \frac{t_{SOCx1,ICE} - t_{SOCx1,x2}}{t_{SOCx1,x2}} \times 100$$

where t_{SOCx1} represents the ignition delay time. The subscript $x1$ represents one of the definitions, maximum oxidation rate of CO to CO_2 (ignition delay referred to CO) or maximum concentration of OH^* (ignition delay referred to OH^*). Finally, the subscript $x2$ represents one of the experimental methods, photo-multiplier or high-speed camera. Of course, only the cases that show OH^* peak in the spectroscopy analysis are taken into account for the calculation of the ignition delay error referred to OH^*, and vice versa.

The average of the errors in absolute value ($\bar{\varepsilon} = \sum \mid \varepsilon \mid /n$), has been calculated for each fuel, as well as its confidence interval with a confidence level of 95 %. The following results are obtained:

- Mean relative error ($\bar{\varepsilon}$) referred to OH^*, between simulations and high speed camera: [0.581, 1.725] % for n-heptane and [1.602, 2.910] % for *iso*-octane.

- Mean relative error ($\bar{\varepsilon}$) referred to CO, between simulations and high speed camera: [1.353, 2.341] % for n-heptane and [1.324, 2.628] % for *iso*-octane.

It is important to mention that the aforementioned errors are cause by deviation in the auto-ignition chemistry and not in the accumulation of excited OH^*. The excited OH sub-model is able to predict with high accuracy

the time at which the OH^* is accumulated (high temperature stage of the autoignition process). Figure 4 shows the time evolution of the normalized OH^* intensity from the high speed camera, as well as the normalized OH^* molar fraction from CHEMKIN and the oxidation of CO to CO_2, for two cases.

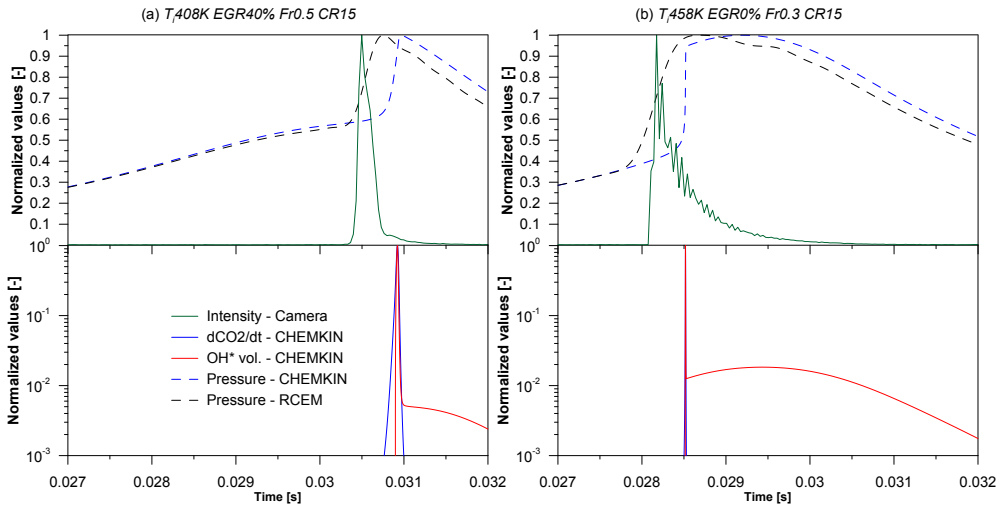

Figure 4: Normalized evolution of the oxidation rate of CO, OH^* molar fraction, integrated natural chemiluminescence intensity from camera, and simulated and experimental pressures for two different cases, with and without OH^* peak in the spectroscopic analysis. Left.- Chemiluminescence belongs to CO continuum. Right.- Chemiluminescence belongs to OH^*.

Figure 4-Left shows a case in which the OH^* radiation is outshined by the CO oxidation; therefore, two different sources of radiation can be measured. On one hand, the luminosity recorded during the combustion belongs to the CO continuum. On the other hand, the decay from $\approx$0.03075 s, which occurs after the combustion, may belong to the OH^* chemiluminescence. Figure 4-

Right shows a case in which the OH^* radiation is dominant; therefore, all the chemiluminescence at 310 nm belongs to this radical. It should be noted that the time of life of the luminosity is much longer since the decay of the OH^* is also gradual. The measured OH^* radiation is consistent with the OH^* predicted by the chemical kinetic mechanism. Both experimental methods show similar profiles, and it can be seen that a short *time of life* of the luminous intensity is directly related with an absence of peak of OH^* in the spectroscopic analysis.

The OH^* intensity is directly related with the amount of accumulated OH^* and with the thermodynamic conditions in the combustion chamber. The higher the reached temperature and the higher the concentration of OH^*, the higher its luminous intensity. The combination of low temperature and small concentration of OH^* is the reason why cool flames are not detected by the photo-multiplier nor by the camera.

Finally, Figure 5 show a comparison between the molar fraction of OH at their ground and excited states for the two cases previously discussed. It can be seen that the peaks take place at the same instant for each of the cases, an instant which corresponds with the pressure rise caused by the ignition (maximum chemiluminescence). Nevertheless, the decay is different for both cases and therefore the time of life for the radiation will also be different than the OH at its ground estate. In this sense a sub-model for the prediction of excited OH is necessary to perform a chemical kinetic analysis of chemiluminescence results.

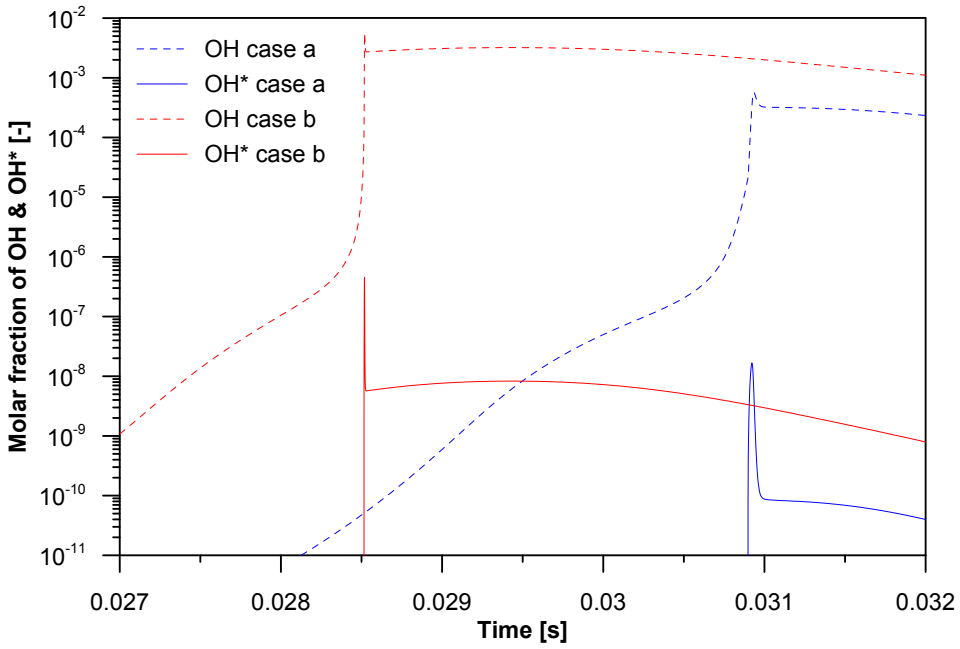

Figure 5: Molar fraction of OH and OH^* for the two different cases Figure 4.

5. Results and discussion

In this section the combustion process is studied from a point of view of spectrography and chemical kinetics. After that, experimental profiles of integrated luminosity and modelled oxidation rate of CO and OH^* accumulation are related.

A spectroscopic analysis was performed to determine the source of the radiation measured by natural chemiluminescence at 310 nm. The results show two different scenarios, which can be seen in Figure 6.

On one hand, for very lean or very low-temperature conditions the spectrum is dominated by the CO continuum, which covers a range of wave-

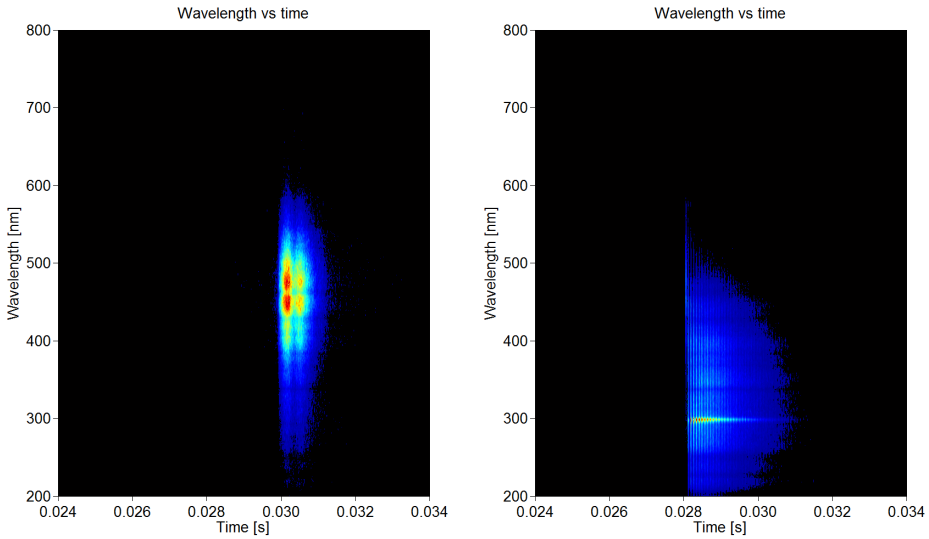

(a) T_i408K $EGR$40 % Fr0.5 $CR$15:1 (b) T_i458K EGR0 % Fr0.3 $CR$15:1

Figure 6: Evolution of the spectrum inside the chamber for two different cases fuelled with *iso*-octane. Left.- without OH^* peak at 310 nm. Right.- with OH^* peak at 310 nm.

lengths from 300 nm to 550 nm. In these cases no peak of intensity can be seen around 310 nm, which implies that the natural chemiluminescence at this wavelength belongs to the CO continuum and it outshines the OH^* radiation. On the other hand, for more intense combustions a clear and long-lasting peak of intensity centered at 310 nm can be identified. Thus, the natural chemiluminescence measured in these cases may belong to OH^*. Therefore, the experiments can be divided in two groups, those that present an OH^* peak in the spectroscopic analysis and those that only show the CO continuum. These groups are shown in Table 4

Figures 7 and 8 show two sequences of images where the evolution of the natural chemiluminescence at 310 nm over time can be seen in terms

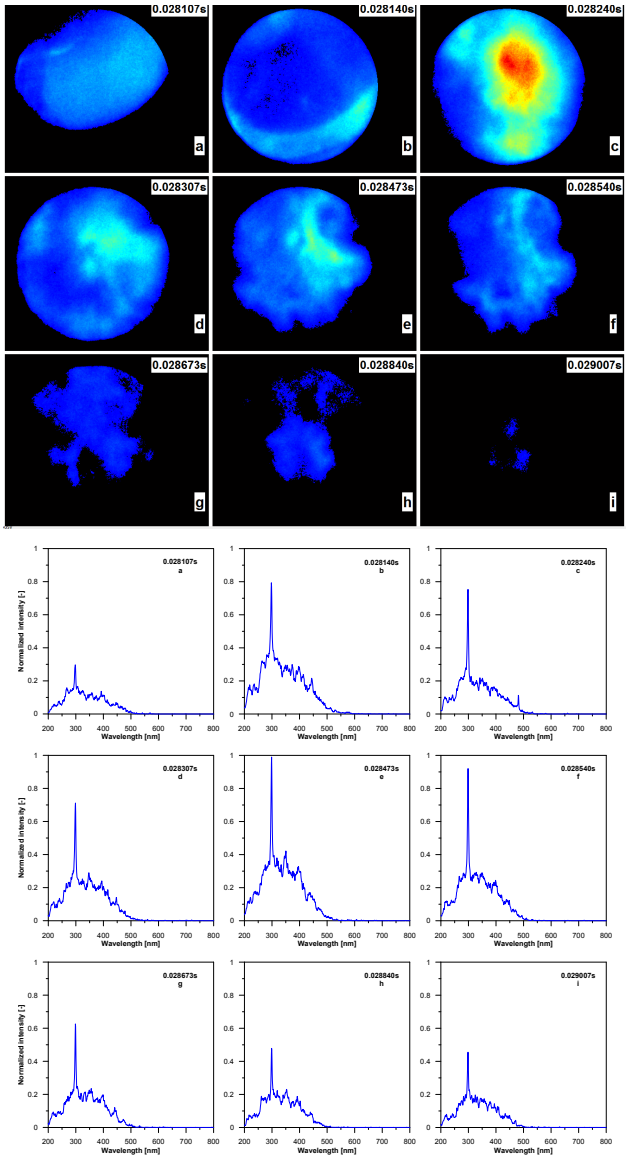

Figure 7: Evolution of chemiluminescence and spectroscopic analysis inside chamber for *iso*-octane at CR 15:1, T_i $458K$, EGR 0 % and Fr 0.3. Top.- OH^* intensity. Bottom.- Spectra.

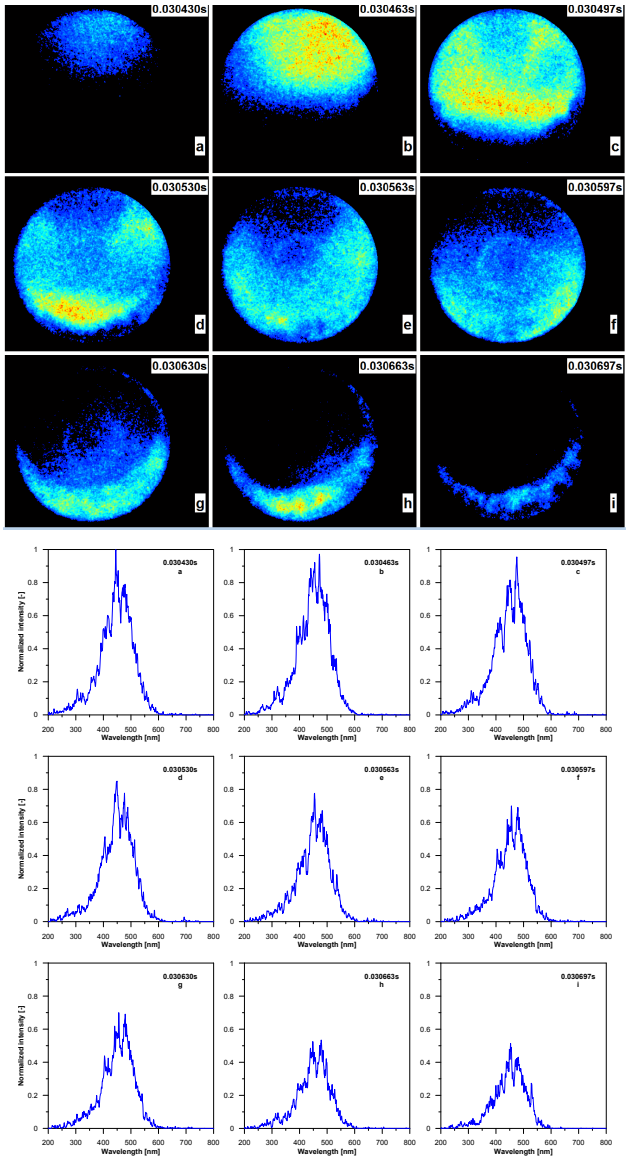

Figure 8: Evolution of chemiluminescence and spectroscopic analysis inside chamber for *iso*-octane at CR 15:1, T_i 408K, EGR 40 % and Fr 0.5. Top.- CO continuum intensity. Bottom.- Spectra.

Fr [-] \ T_i [K]	358	383	408	433	458
0.3	40		0, 30, 40, 50		40
0.4	0, 30, 40, 50	40, 50	0, 30, 40, 50	40, 50	0, 30, 40, 50
0.5	40	40	40, 50	40	40
0.6	40		40, 50		40
0.7			40, 50		
0.8			40, 50		

Table 4: Parametric study performed. Green.- cases in which there is a peak of OH^*. Black.- cases in which the CO continuum outshines the OH^*.

of intensity and area. Besides, the spectra of the combustion chamber are also showed for each time of the sequences. It can be clearly seen in Figure 7 a peak of OH^* in the spectrum of the combustion which means that the chemiluminescent radiation measured belongs to the OH^* radical. However, the absence of a peak in the spectrum of Figure 8 implies that the measured chemiluminescence belongs to CO. Additionally, by linking the information provided with Figure 4 the auto-ignition and combustion process can be described as follows:

i For two-stage ignitions, the so called cool flames start appearing and a small peak in the pressure rise rate can be seen (Figure 2). There is a tiny amount of radicals generated, which added to the low temperature are not enough to generate significant luminosity. In fact, a really small amount of OH^* is accumulated according to the validated sub-model, being the main formation reaction of such radi-

cal $HO_2 + H \Rightarrow OH + OH^*$. However, HO_2 has an accumulation behavior during cool flames and the relevance of the previous reaction is negligible. Moreover, the exited OH^* that is formed during this stage reacts with the CH_3 through the third body reaction $CH_3 + OH^* + M \Rightarrow CH_3OH + M$. Therefore, no decay of exited OH to its ground state is present and no radiation is emitted.

ii With the start of the NTC phase there is a decrease in reactivity as the formation of chain carriers and formation of olefins are competing against each other; causing a change of slope in the pressure curve (Figure 2). Almost all the exothermic reactions are frozen during this stage, including the generation and decay of OH^*. Thus, no radiation can be seen during the NTC zone.

iii The NTC stage comes to an end due to a slight increase in temperature. This phase is controlled by the decomposition of H_2O_2 through a third-body reaction $H_2O_2 + M \Rightarrow 2OH + M$. There is still no presence of OH^* chemiluminescence as the OH generated is consumed to oxidize formaldehyde into CO instead of forming excited OH^*. At this point the heat release starts.

iv After its formation, the CO starts to oxidize into CO_2. The oxidation of CO is mainly caused by OH through $CO + OH \Rightarrow CO_2 + H$ and by O through $CO + O \Rightarrow CO_2 + hv$ (which is a luminous reaction). Therefore, the so called CO continuum starts. This light emission covers a range of wavelengths from 300 nm to 550 nm and, if it is bright enough, it can outshine the OH^* chemiluminescence.

At the same time, the OH accumulation starts through the reactions $O + H_2O \Rightarrow 2OH$ and $H + O_2 \Rightarrow O + OH$. The appearance of excited OH^* is promoted by the accumulation of OH and the chemiluminescence radiation starts. Light is emitted by the decay of OH^* to its ground state mainly thanks to its reaction with O_2, CO, CO_2, H_2O and N_2 ($OH^* + M \Rightarrow OH + M$). H2O is the dominant third body species whereas N2 is the less relevant due to the higher activation energy of its reaction. At the end of this phase the pressure rise rate reaches a peak (Figure 4) and it is in this instant where the chemiluminescence takes up the whole chamber (Figures 7-c and 8-c).

Two different scenarios can be present at this stage. For lean equivalence ratios or low-temperature conditions the accumulated OH^* is not enough and the natural chemiluminescence at 310 nm belongs to the CO continuum, since no peak can be seen at this wavelength (Figure 8-Bottom). However, for higher combustion temperatures the active compound H formed during the oxidation of CO terminates with the radical HO_2 (last chain carrier to disappear) through $H + HO_2 \Rightarrow 2OH$. The increase of relevance of this reaction at high combustion temperatures causes a higher OH^* accumulation, which leads to a brighter OH^* emission. In this case, a peak of intensity can be seen at 310 nm (Figure 7-Bottom), which means that the natural chemiluminescence at this wavelength belongs to OH^*.

v Once all the CO has been oxidized into CO_2 the maximum cycle pressure is reached and the heat release stops (Figure 4). For the cases in which the CO continuum predominates, this instant coincides with

the end of the light emission (Figure 8-i). However, for the cases that show peak of OH^*, significant amounts of this radical remains in the combustion chamber and the luminous intensity continues during part of the expansion (Figure 7-h).

vi Finally, the excited OH^* disappears and the chemiluminescence of OH stops. Since the OH radical is only stable at high temperatures, it also disappears during the expansion stroke (Figure 7-i) by its recombination with atomic oxygen, $OH + O \Rightarrow O_2 + H$.

The oxidation of CO and the accumulation of OH^* occur simultaneously. Therefore, a priori, it is not possible to decide without a spectrograph if the natural chemiluminescence at 310 nm belongs to OH^* or if it is outshined by the CO continuum. However, it should be noted that the *time of life* of the luminous intensity is very different in case of belonging to CO continuum or to OH^*, as can be seen in Figure 4, where the *time of life* of the OH^* chemiluminescence is 0.65 ms longer than the CO continuum luminosity. Thus, it is possible to use this parameter as a criterion to determine the source of the radiation.

6. Conclusions

The auto-ignition process and phases of combustion under HCCI combustion conditions using PRFs have been studied in a RCEM by means spectroscopy. The experimental results have also been used to validate a chemical kinetic mechanism for *n*-heptane and *iso*-octane and a sub-model for the excited OH. Additionally, the different combustion phases have been

analyzed by measuring the chemiluminescence of OH^* and CO and the results have been contrasted with those of the chemical kinetics. Last, the experimental results of radiation have also been related to the simulations.

The following conclusions can be deducted from this study:

- The experimental ignition delay times have been reproduced with the chemical kinetic mechanism. Additionally, the different definitions of ignition delay are able to be reproduce, such as: Maximum pressure rise, maximum concentration of OH, and maximum oxidation rate of CO.

- The spectroscopic analysis showed that there were two types of emission; one dominated by the CO continuum and another from the OH^*. The CO was seen to appear at lean equivalence ratios and low temperatures, while on the other hand, the OH^* was present at high combustion temperatures. Reaction $H + HO_2 \Rightarrow 2OH$ becomes more relevant at high combustion temperatures, which causes high accumulation of OH^* and therefore higher luminosity. Additionally, the fuel also showed a big influence on the type of luminosity generated. The cases with *iso*-octane presented a more violent combustion which lead to the generation of more OH^*, whereas the luminous emission from cases with n-heptane was more prone to be dominated by the CO continuum. Therefore, the cases can be separated into two groups (OH^* and CO) based on the contour conditions and fuel employed.

- Neither of the optical techniques applied (chemiluminescence nor spectroscopy) were able to detect the *cool flames*. This was because either

the in-cylinder temperature was too low or the the accumulated OH^* concentration was too little. The luminous intensity of the OH^* radical started when the CO began oxidizing into CO_2, before the generated OH was consumed by the generation of CO. The time of maximum pressure rise rate was coincidental with that of the the maximum radiation, which also took place very close to the maximum oxidation rate of the CO to CO_2. And last, OH^* radical disappeared during the expansion stroke as it was only stable at high temperatures.

- Separating the chemiluminescence emitted by the accumulation of the OH^* radical from that coming from the oxidation of CO to CO_2 was a difficult task to accomplish just by using natural chemiluminescence measurements at 310 nm. However, given the different *time of life* of each of the species, where that corresponding the CO is shorter than the one of OH^*, it was found that the *time of life* was an appropriate indicator of the origin of the luminosity detected being longer for the cases in which the OH^* dominates the radiation.

Acknowledgements

The authors would like to thank different members of the LAV team of the ETH-Zürich for their contribution to this work. The authors are grateful to the Universitat Politècnica de València for financing the Ph.D. Studies of W.Vera-Tudela (FPI SP1 grant 30/05/2012) and his stay at ETH-Zürich (grant 30/12/2014). Finally, the authors would like to thank the Spanish Ministry of Education for financing the Ph.D. Studies of Darío López-Pintor (grant FPU13/02329) and his stay at ETH-Zürich (grant EST14/00626).

Nomenclature

Abbreviations

BDC	Bottom dead center
CI	Compression ignition
CR	Compression ratio
EGR	Exhaust gas recirculation
$FWHM$	Full width at half maximum
$HCCI$	Homogeneous charge compression ignition
ICE	Referred to data obtained from CHEMKIN using the internal combustion engine reactor
LTC	Low temperature combustion
NTC	Negative temperature coefficient
$PCCI$	Premixed charge compression ignition
PHM	Photo-multiplier
PRF	Primary reference fuel
$RCEM$	Rapid compression expansion machine
SI	Spark ignition

TDC	Top dead center
UHC	Unburned hydrocarbons

Greek letters

ϵ	Percentage error in ignition delay referred to the maximum pressure rise between experimental and simulation results
$\bar{\epsilon}$	Mean relative error in ignition delay referred to the maximum pressure rise between experimental and simulation results
ε	Percentage error in ignition delay referred to the peak of OH^* or maximum oxidation rate of CO between experimental and simulation results
$\bar{\varepsilon}$	Mean relative error in ignition delay referred to the peak of OH^* or maximum oxidation rate of CO between experimental and simulation results

Roman letters

P	Air pressure
T	Air temperature
t	Time
Fr	Working equivalence ratio
Y	Mass fraction

Subscripts

i	corresponding to the initial conditions
ICE	corresponding to the simulations with CHEMKIN using a 0D ICE reactor
O_2	corresponding to the oxygen specie
$RECEM$	corresponding to the experimental results from the RCEM
SOC	corresponding to the start of combustion
TDC	corresponding to the top dead center
$x1$	corresponding to either the simulated maximum oxidation rate of CO to CO_2 or maximum concentration of OH^*

$x2$	corresponding to either the experimental measurements from the photo-multiplier or the high-speed camera

Superscripts

$*$	corresponding to the excited state of an element

Appendix A. Excited OH sub-model

The excited OH sub-model is composed by two blocks of reactions. On one hand, some reactions of the Curran chemical kinetics mechanism have been modified in in order to distinguish the ground state OH from the excited state one (OH^*) maintaining the same specific reaction rates of the original mechanism [26, 27]. On the other hand, the Hall and Petersen sub-model for the OH^* has been taken into account. The specific reaction rate of each reaction can be found in the corresponding reference [13]. All 22 reactions where the OH^* is involved are shown below.

	Reaction	Reference
1	$CH + O_2 \Leftrightarrow CO + OH^*$	[13]
2	$H + O + M \Leftrightarrow OH^* + M$	[13]
3	$H + 2OH \Leftrightarrow OH^* + H_2O$	[13]
4	$OH^* + Ar \Leftrightarrow OH + Ar$	[13]
5	$OH^* + H_2O \Leftrightarrow OH + H_2O$	[13]
6	$OH^* + CO_2 \Leftrightarrow OH + CO_2$	[13]
7	$OH^* + CO \Leftrightarrow OH + CO$	[13]
8	$OH^* + H \Leftrightarrow OH + H$	[13]
9	$OH^* + H_2 \Leftrightarrow OH + H_2$	[13]
10	$OH^* + O_2 \Leftrightarrow OH + O_2$	[13]
11	$OH^* + O \Leftrightarrow OH + O$	[13]
12	$OH^* + OH \Leftrightarrow OH + OH$	[13]
13	$OH^* + CH_4 \Leftrightarrow OH + CH_4$	[13]
14	$OH^* + N_2 \Leftrightarrow OH + N_2$	[13]
15	$OH^* \Leftrightarrow OH + hv$	[13]
16	$CH_4 + O \Leftrightarrow CH_3 + OH^*$	[29]
17	$O + H_2 \Leftrightarrow H + OH^*$	[29]
18	$O + H_2O \Leftrightarrow OH + OH^*$	[29]
19	$CH_3OH + M \Leftrightarrow CH_3 + OH^* + M$	[29]
20	$NH_3 + O \Leftrightarrow NH_2 + OH^*$	[29]
21	$HO_2 + O \Leftrightarrow OH^* + O_2$	[30]
22	$HO_2 + H \Leftrightarrow OH + OH^*$	[30]

References

[1] N.P. Komninos. The effect of thermal stratification on HCCI combustion: A numerical investigation. *Applied Energy*, 139:291–302, 2015.

[2] J. Rezaei, M. Shahbakhti, B. Bahri, and A.A. Aziz. Performance prediction of HCCI engines with oxygenated fuels using artificial neural networks. *Applied Energy*, 138:460–473, 2015.

[3] A.P. Singh and A.K. Agarwal. Combustion characteristics of diesel HCCI engine: An experimental investigation using external mixture formation technique. *Applied Energy*, 99:116–125, 2012.

[4] C. Fang, F. Yang, M. Ouyang, G. Gao, and L. Chen. Combustion mode switching control in a HCCI diesel engine. *Applied Energy*, 110:190–200, 2013.

[5] D. Jung and N. Iida. Closed-loop control of HCCI combustion for DME using external EGR and rebreathed EGR to reduce pressure-rise rate with combustion-phasing retard. *Applied Energy*, 138:315–330, 2015.

[6] R. Augusta, D.E. Foster, J.B. Ghandhi, J. Eng, and P.M. Najt. Chemiluminescence measurements of homogeneous charge compression ignition (HCCI) combustion. In SAE Technical Papers, editor, *2006 SAE World Congress*, Detroit, MI; United States, 3 2006. Code 90162.

[7] H.F. Liu, M.F. Yao, C. Jin, P. Zhang, Z.M. Li, and Z.Q. Zheng. Chemiluminescence spectroscopic analysis of homogeneous charge compression ignition combustion processes. *Spectroscopy and Spectral Analysis*, 30:2611–2615, 2010.

[8] E. Mancaruso and B.M. Vaglieco. Spectroscopic measurements of premixed combustion in diesel engine. *Fuel*, 90:511–520, 2011.

[9] ASME-JSME, editor. *A spectroscopic analysis of combustion in homogeneous charge compression ignition engine*, Vancouver, British Columbia, CANADA, 7 2007. ASME-JSME Thermal Engineering Summer Heat Transfer Conference. HT2007-32552.

[10] B. Kim, M. Kaneko, Y. Ikeda, and T. Nakajima. Detailed spectral analysis of the process of HCCI combustion. *Proceedings of the Combustion Institute*, 29:671–677, 2002.

[11] E. Murase, K. Hanada, T. Miyaura, and J. Ikeda. Photographic observation and emission spectral analysis of homogeneous charge compression ignition combustion. *Combustion Science and Technology*, 177:1699–1723, 2005.

[12] W. Hwang, J. Dec, and M. Sjï¿½berg. Spectroscopic and chemical-kinetic analysis of the phases of HCCI autoignition and combustion for single- and two-stage ignition fuels. *Combustion and Flame*, 154:387–409, 2008.

[13] J.M. Hall and E.L. Petersen. An optimized kinetics model for OH chemiluminescence at high temperatures and atmospheric pressures. *International Journal of Chemical Kinetics*, 38:714–724, 2006.

[14] M. Sjoberg and J.E. Dec. Isolating the effects of fuel chemistry on combustion phasing in an HCCI engine and the potential of fuel stratification for ignition control. *SAE Technical Paper*, 2004-01-0557, 2004.

[15] J. M. Desantes, J. J. López, S. Molina, and D. López-Pintor. Numerical simulation of autoignition of gasoline-ethanol/air mixtures under different conditions of pressure, temperature, dilution, and equivalence ratio. *SAE Technical Paper*, 2011-01-0341, 2011.

[16] J. M. Desantes, J. J. López, S. Molina, and D. López-Pintor. Validity of the livengood & wu correlation and theoretical development of an alternative procedure to predict ignition delays under variable thermodynamic conditions. *Energy Conversion and Management*, 105:836–847, 2015.

[17] D. Mitakos, C. Blomberg, Y. Wright, P. Obrecht, B. Schneider, and K. Boulouchos. Integration of a cool-flame heat release rate model into a 3-stage ignition model for HCCI applications and different fuels. *SAE Technical Paper*, 2014-01-1268, 2014.

[18] G. Barroso, A. Escher, and K. Boulouchos. Experimental and numerical investigations on HCCI combustion. *SAE Technical Paper*, 2005-24-038, 2005.

[19] D. Mitakos, C. Blomberg, A. Vandersickel, Y. Wright, B. Schneider, and K. Boulouchos. Ignition delays of different homogeneous fuel-air mixtures in a Rapid Compression Expansion Machine and comparison with a 3-stage-ignition model parametrized on shock tube data. *SAE Technical Paper*, 2013-01-2625, 2013.

[20] S. Schlatter, B. Schneider, Y. Wright, and K. Boulouchos. Comparative study of ignition systems for lean burn gas engines in an optically accessible Rapid Compression Expansion Machine. *SAE Technical Paper*, 2013-24-0112, 2013.

[21] T. Steinhilber and T. Sattelmayer. The effect of water addition on HCCI diesel combustion. *SAE Technical Paper*, 2006-01-3321, 2006.

[22] S. Schlatter, B. Schneider, Y. Wright, and K. Boulouchos. Experimental study of ignition and combustion characteristics of a diesel pilot spray in a lean premixed methane/air charge using a Rapid Compression Expansion Machine. *SAE Technical Paper*, 2012-01-0825, 2012.

[23] G. Woschni. A universally applicable equation for the instantaneous heat transfer coefficient in the internal combustion engine. *SAE Technical Paper*, 670931, 1967.

[24] J. Benajes, P. Olmeda, J. Martï¿½n, and R. Carreï¿½o. A new methodology for uncertainties characterization in combustion diagnosis and thermodynamic modelling. *Applied Thermal Engineering*, 71:389–399, 2014.

[25] F. Payri, S. Molina, J. Martï¿½n, and O. Armas. Influence of measurement errors and estimated parameters on combustion diagnosis. *Applied Thermal Engineering*, 26:226–236, 2006.

[26] H.J. Curran, P. Gaffuri, Pitz W.J, and C.K. Westbrook. A comprehensive modeling study of n-heptane oxidation. *Combustion and Flame*, 114:149–177, 1998.

[27] H.J. Curran, P. Gaffuri, W. J. Pitz, and C. K. Westbrook. A comprehensive modeling study of iso-octane oxidation. *Combustion and Flame*, 129:253–280, 2002.

[28] H.J. Curran, W.J. Pitz, C.K. Westbrook, C.V. Callahan, and F.L. Dryer. Oxidation of automotive primary reference fuels at elevated pressures. *Proceedings of the Combustion Institute*, 27:379–387, 1998.

[29] C.H. Bamford, R.G. Compton, and C.F.H. Tipper. *The Formation and Decay of Excited Species*. Elsevier Science, 1 edition, 1 1969.

[30] S.T. Lunt, G. Marston, and R.P. Wayne. Formation of $O_2(a^1\Delta_g)$ and vibrational excited OH in the reaction between O atoms and HO_x species. *Journal of the Chemical Society, Faraday Transactions 2: Molecular and Chemical Physics*, 84(7):899–912, 1988.